文章编号：0258-8013 (2012) S1-0475-09　　中图分类号：TM 341；TM 359　　文献标志码：A　　学科分类号：470·40

U 型永磁同步直线电机气隙磁场优化设计

孙鹏，周惠兴

(中国农业大学工学院，北京市 海淀区 100083)

Air-gap Magnetic Field Optimization for U-shaped Ironless Permanent Magnet Linear Synchronous Motors

SUN Peng, ZHOU Huixing

(College of Engineering, China Agricultural University, Haidian District, Beijing 100083, China)

ABSTRACT: A U-shaped ironless permanent magnet linear synchronous motor was studied in this paper. In order to achieve desirable performance, the air-gap flux density distribution was taken as the primary problem. A design optimization was proposed to yield improvement in the thrust amplitude and reduction in the thrust ripple and magnetic material consumption. A multiobjective optimization solver using genetic algorithm was employed to find the optimal motor dimensions. The design optimization was verified by a layered finite element analysis, which could lower the complexity of the magnetic field analysis. The effectiveness of the proposed idea was further confirmed by experimental results of the prototype, which demonstrated reasonable agreement with the analytical solution.

KEY WORDS: permanent magnet linear synchronous motor; air-gap flux density distribution; layer model; multiobjective optimization; layered finite element analysis

摘要：以 U 型无铁心永磁同步直线电机的气隙磁场分布为研究对象，引入层模型理论分析，针对增大电机推力密度，降低推力波动和降低永磁体使用的实际需求，提出了多目标优化设计方案，以同时实现上述目标。运用遗传算法来选取最佳的电机尺寸。在传统有限元法的基础上，提出三维分层有限元法，能在保证磁场分析正确性的同时，降低分析难度。仿真表明与理论分析结果相吻合，证明了所提出的三维分层有限元法的准确性，样机试验结果进一步验证了所提多目标优化设计方案和三维分层有限元的有效性。

关键词：永磁同步直线电机；气隙磁场分布；层模型；多目标优化设计；三维分层有限元

0 INTRODUCTION

Modern mechanical systems, such as machine tools, semiconductor manufacturing, laser cutting, robot manipulators, and automatic inspection machines, often require high speed and high accuracy linear motions. These linear motions are usually realized using rotary motors with mechanical transmission mechanisms such as reduction gears and lead screws. Such mechanical transmissions not only significantly reduce linear motion speed and dynamic response, but also introduce backlash, large frictional and inertial loads, and structural flexibility [1-2]. As an alternative, the direct drive permanent magnet linear synchronous motor (PMLSM) is probably the most naturally applicable in these high speed and high accuracy positioning systems. Usually, the iron-core PMLSM among various linear motor types attracts more attraction because of the higher developed thrust density and higher efficiency as well as high dynamic performance [3]. However it is subject to significant force ripple. These uncertain nonlinearities are directly transmitted to the load and thus have significant effect on its motion performance.

It seems that two ways can be adopted in order to achieve the potential high performance of the PMLSM. On the one hand, many control strategies have been developed. For example, authors in [2,4-5] presented an nonlinear adaptive robust control scheme for high speed and high accuracy motion control of linear motors, where on-line parameter adaptation and certain robust control laws were used to reduce the effect of various parameter uncertainties and handle the uncompensated uncertain nonlinearities. However

基金项目：国家建设高水平大学公派研究生项目(2009635005)。

This work was supported in part by the China Scholar Council under the State Scholarship Fund (2009635005).

on the other hand, one can reduce the force ripple by proper motor design before adopting sophisticated control strategies to counteract the downside of iron-core PMLSM.

Recently, a specific type of linear motor, namely, the U-shaped ironless PMLSM (UIPMLSM) has been rapidly developed and gains attentions of engineers [6-8]. The UIPMLSM has advantages such as lack of cogging force, no attracting force between the armature (or named as forcer) and the permanent magnets, and negligible iron loss, because it has symmetrical topologies of magnets and lacks primary iron core and teeth, as shown in Fig. 1. However, there are still several factors that result in undesirable performance and high manufacturing cost, such as lower thrust density, relatively low thrust ripple, and larger non-ferromagnetic air gap which requires more permanent-magnet (PM) material. The manufacturing cost can be reduced by decreasing PM consumption. The thrust ripple in an UIPMLSM is mainly produced by nonsinusoidal distribution of PM and armature magnetic fields. With a fixed coil structure, thrust ripple can be reduced by a reduction of PM field harmonics. Actually, in the areas that need precise position control, the applied UIPMLSM must have sinusoidal air-gap flux density distribution waveforms because the thrust ripple could be controlled little enough if winding currents are also sinusoidal in the meantime [6, 9-10]. Furthermore the air-gap flux density distribution of PM poles also has a significant effect on the thrust density through the development of thrust.

Thus, during the past decade, significant efforts have been devoted to solving the difficulties in shaping such an air-gap flux density distribution as close to a sinusoidal waveform as possible. Among them, authors in [11-13] applied the multi-pole Halbach array magnetized topology which has a self-shielding property and higher flux density than vertically magnetized topology. However, this method not only needs many PM pieces with different dimensions, but also requires a complex magnetization system and procedure, which increases the complexity and cost of PM pieces manufacture and motors assembly. The magnet arc shaping technique was presented in [10, 14] to achieve the sinusoidal back EMF waveforms. However, this method suffers from non-uniform air gap and also increases the complexity and cost of PM pieces manufacture and motors assembly. Moreover the PM material is not fully utilized in the pole ends. In [15], a modular PM poles configuration was proposed to shape the air-gap flux density distribution. This configuration consists of three or more PM pieces of different quality, which also increases the complexity and cost of PM poles assembly.

On the other hand, an effective method is to eliminate one or more harmonics by adjusting the dimensions of PM poles with conventional array. This proposed method develops a high thrust and a substantially reduced thrust pulsation, resulting in desirable motor performance. The use of PM pieces with same dimensions also takes economic factors into account by reducing the complexity and cost of manufacturing PM pieces and assembling motors.

In this paper, we take the air-gap flux density distribution as a primary problem in the motor design optimization with a fixed coil structure. At first, a layer model is introduced in defining the optimization problem. Then, a multiobjective function with appropriate constraints is defined to increase the air-gap magnetic flux density amplitude, reduce the higher harmonics of air-gap magnetic flux density distribution, and decrease the PM volume. The PM dimensions and air-gap length are chosen as design variables. A multiobjective optimization solver using genetic algorithm is employed to search for optimal design values. The layered finite element analysis (LFEA) is developed to reduce the complexity and time-consumption of three-dimensional finite element analysis (3DFEA) and to verify the effectiveness of proposed method. Finally, a motor prototype with optimized dimensions is built for experiments to further validate the air-gap magnetic field design optimization.

1 LAYER MODEL OF THE UIPMLSM

1.1 Structure of the UIPMLSM

Fig. 1 (a) shows a schematic diagram of the

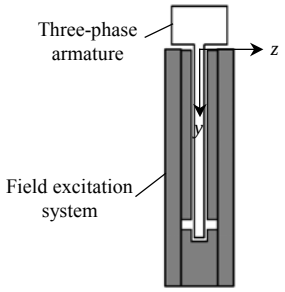

(a) 侧视结构图

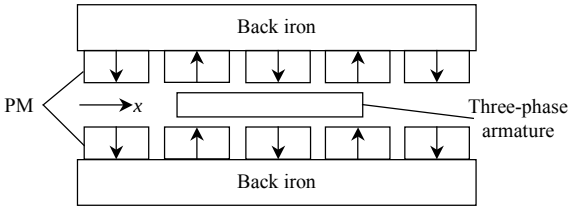

(b) 正视结构图

图 1　U 型永磁同步直线电机结构图

Fig. 1　Schematic diagram of the UIPMLSM

UIPMLSM studied in this paper. It consists of the external U-shaped PM field excitation system and the internal three-phase armature.

The U-shaped PM field excitation system is composed of back irons, which looks like a capital letter U, and face-to-face surface-type PM pieces. The back iron is ferromagnetic. The PM pieces are magnetized in the normal direction and mounted on the internal surface of the U-shaped yoke, facing the armature and arranging equably with symmetrical topologies and staggered magnetic poles N, S, … N, S, as shown in Fig. 1 (b). The three-phase armature is an ironless winding layer in which the input current waveforms are sinusoidal. In this paper, we assume the coil structure is fixed.

Similar as the permanent magnet rotary synchronous motors, the thrust (named torque in rotary motors) is generated by the interaction between the permanent magnetic field and the traveling magnetic field, while the synchronous speed of the motor is the same as the speed of the traveling magnetic field [3].

In the middle of air gap, the direction along the motion of ironless armature is defined as longitudinal (x) axis and the direction along the motor width is defined as transverse (y) axis. And the direction perpendicular to the x-y plane is defined as normal (z) axis. Here, the x, y, and z coordinates compose the Cartesian coordinate system, as shown in Fig. 1.

1.2　Layer Model of the UIPMLSM

Fig. 2 shows the layer model of the UIPMLSM. In this model, we assume that all regions are extended infinitely in $\pm x$ direction, actually we can realize it by concatenate stators in series. As the permeability of the not excited winding layer is the same as the air layer, we regard them as an integrative air/winding layer when analyzing the magnetic fields due to U-shaped PM field excitation system. Under the assumption of infinite permeability of the back iron, the domain of the motor is quite simple [16]. Thus only two regions are considered for the magnetic field analysis in this analytical model. Layer I and II in Fig. 2 represent the air/winding region and the permanent magnet region respectively.

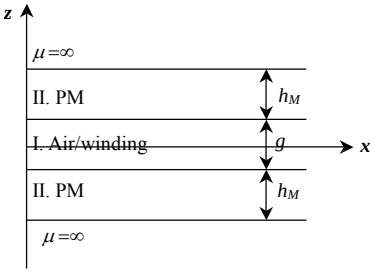

图 2　U 型永磁同步直线电机层模型

Fig. 2　Layer Model of the UIPMLSM

Assuming no variation along the y-axis, the problem can be simplified to a two-dimensional field distribution where the air-gap flux density has only two components, i.e., longitudinal component B_x and normal component B_z. And the air-gap flux density can be predicted by solving the Laplace's (for layer I) and Poisson's (for layer II) equations [6, 13, 17]. In this paper, we assume that the magnetic flux density in the middle of air gap is sinusoidal with some higher harmonics and the magnetic saturation is neglected. Therefore, the B_z can be obtained as

$$B_z = \frac{\partial A}{\partial x} = -\sum_{n=1,3,\cdots}^{\infty} C\frac{2n\pi \mathrm{e}^{-n\pi g/(2\tau)}}{\tau}\cos(\frac{n\pi x}{\tau}) \qquad (1)$$

where $\boldsymbol{A}$ is the magnetic vector potential in the air/winding layer, τ is the pole pitch, g is the air-gap length, and n is the harmonics order. The constant C is given by

$$C=\frac{\dfrac{4B_r\pi}{(n\pi)^2}\sin\dfrac{n\eta\pi}{2}}{(a+1)+\dfrac{\mu_M(a-1)(b+1)}{\mu_0(b-1)}} \qquad (2)$$
$$a=\mathrm{e}^{-n\pi g/\tau},\quad b=\mathrm{e}^{-2n\pi h_M/\tau}$$

where B_r is the remanence of the PM, μ_M is the permeability of the PM, μ_0 is the permeability of free space, η is the ratio of magnet width to pole pitch, and h_M is the height of a PM piece.

2 MULTIOBJECTIVE OPTIMIZATION

The design objectives in this paper are aim to improve the undesirable performance by increasing the thrust density and reducing the thrust ripple and the manufacturing cost. Therefore, we need to identify the functional relations between these objectives and the design variables.

First of all, the B_z is described in Eq. (1). With a fixed coil structure, the motor developed thrust is directly proportional to the B_z. Thus, the B_z can be employed as an indirect measure of the developed thrust. The optimization procedure is employed to maximize the B_z.

The second design objective is to shape the air-gap flux density distribution close to sinusoidal form. The thrust ripples can be reduced by reduction of higher flux harmonics. Therefore, the total harmonic distortion (THD) of flux density distribution is employed as an indirect measure of the thrust ripple as

$$F_r=\sqrt{\sum_{n=3,5,7,\cdots}^{\infty}B_{ng}^2}\,/\,B_{1g} \qquad (3)$$

where B_{ng} is the nth harmonics of air-gap magnetic flux density distribution. As for three phase winding, the 3kth (k=1,3,5,…) harmonics don't influence the motor performance. The optimization procedure is employed to minimize the THD.

The third design objective is to reduce the production cost. It can be reduced by decreasing PM consumption and using PM pieces with same dimensions. For face-to-face surface-type PM pieces, the volume of PM pieces is obtained as

$$V_M=2p\times l_M\times w_M\times h_M \qquad (4)$$

where p is the number of pole pairs. The l_M, w_M and h_M stand for the length, width, and height of one PM piece respectively. The optimization procedure is employed to minimize the V_M.

Considering what have mentioned above, the multiobjective optimization problem is formulated as a vector of three objectives

$$\begin{cases}F(\boldsymbol{\theta})=\left[-\left|B_z\right|,\left|F_r\right|,V_M\right]\\ \text{Min}\ F(\boldsymbol{\theta})=\begin{cases}\text{Max}\left|B_z(\boldsymbol{\theta})\right|\\ \text{Min}\left|F_r(\boldsymbol{\theta})\right|,\\ \text{Min}V_M(\boldsymbol{\theta})\end{cases}\quad \boldsymbol{\theta}\in R^n\end{cases} \qquad (5)$$

where $\boldsymbol{\theta}$=[l_M, w_M, h_M, g] is the vector of design variables, B_z, F_r and V_M stand for the thrust density, the thrust ripple function and the PM volume, respectively. This vector of objectives must be traded off in some way. The relative importance of these objectives is not generally known until the system's best capabilities are determined and trade-offs between objectives are fully understood [6,18-19]. The designers must rely on their intuition and ability to express preferences throughout their own specific optimization cycle. Some principal values have been fixed for each motor design, which are listed in Tab. 1.

表 1 U 型永磁同步电机基本参数

Tab. 1 Principal data of the UIPMLSM

Parameters	Value
Pole pitch τ/mm	16
Number of phases m	3
Number of coils per pole per phase q	1
PM type	48H
Remanence of the PM B_r/T	1.40
Inside coercive force of the PM H_c/(kA/m)	995

The genetic algorithm (GA) has been widely used to find the optimal design variables [15, 18, 20-22]. The GA is a method for solving both constrained and unconstrained optimization problems which is based on natural selection. The GA repeatedly modifies a population of individual solutions. At each step, the GA uses three main types of rules at each step: selection rules select the individuals that contribute to the population at the next generation, crossover rules combine two parents to form children for the next generation, and mutation rules apply random changes to individual parents to form children. The selection function chooses parents

for the next generation based on their scaled values from the fitness scaling function. Over successive generations, the population evolves toward an optimal solution. The flowchart of GA is shown in Fig. 3.

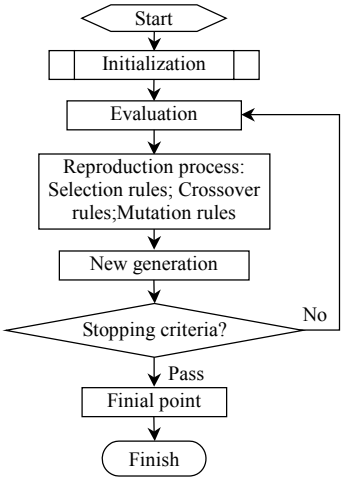

图 3　遗传算法流程表

Fig. 3　Flowchart of the genetic algorithm

The constraints limiting design variables should be taken into account during optimization process to prevent the possibility of reaching unrealistic results. The multiobjective optimization solver using GA with constraints listed in Tab. 2 and parameters listed in Tab. 3 is employed to implement the algorithm. The score diversity of this multiobjective function is shown in Fig. 4.

Here, more emphasis is placed on the amplitude of air-gap magnetic flux density and PM consumption rather than the thrust ripple. The selected results of the

表 2　优化设计变量的限值

Tab. 2　Design variables constraints

Parameter	Symbol	Min/m	Max/m
Length of PM	l_M	0.070	0.110
Width of PM	w_M	0.007	0.016
Height of PM	h_M	0.003	0.007
Air gap length	g	0.006	0.012

表 3　遗传算法参数

Tab. 3　Genetic algorithm parameters

Parameter	Value
Population size	100
Selection function	Tournament
Crossover fraction	0.8
Mutation function	Constraint dependent
Crossover function	Scattered
Stall generations	800

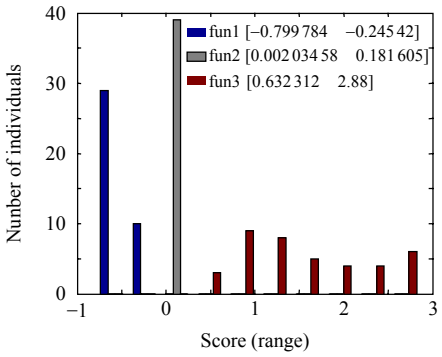

图 4　多目标函数运算取值分布

Fig. 4　Score diversity of the multiobjective function

design optimization are listed in the fourth column of Tab. 4. As a comparison, the specifications of the original motor are list in the third column. The original motor WM-12875 bought from Winnermotor Co., Ltd. (Zhengzhou, China) is wieldy used in education instruments and industrial applications, such as precision motion demo platform, direct driven inverted pendulum, linear motor driven gantry, hardware-in-loop control system, and LED fully-automatic gold wire bonder equipment [23-25]. From Tab.4 it can be seen that the multiobjective optimization design increases the amplitude of air-gap magnetic flux density by 17.2% and decreases the PM volume and thrust ripple function by 29.4% and 9.2% respectively with respect to the original motor.

表 4　优化设计技术参数

Tab. 4　Specifications of optimization design

Parameter	Symbol	Original/m	Optimized/m	Unit
Magnet length	l_M	0.110 0	0.075 0	m
Magnet width	w_M	0.015 0	0.013 6	m
Magnet height	h_M	0.004 0	0.005 0	m
Air gap length	g	0.007 0	0.006 0	m
Amplitude	B_z	0.646 3	0.757 4	T
Ripple function	F_r	0.096 9	0.088 7	1
PM volume	V_M	2.64×10^{-5}	2.04×10^{-5}	m^3

3　LFEA

3.1　Definition of the LFEA

As one of numerical methods in magnetic field analysis, the finite element method is known as an accurate analysis method which can consider geometric details and the nonlinearity of magnetic material. The two-dimensional FEA is easy to build the model and fast to compute, however is not

accurate enough as that in the 3DFEA. On the other hand the 3DFEA is accurate, however is complex and requires long computation time especially at the initial design stage. Therefore, a layered finite element analysis (LFEA) is developed to bridge the gap between these two approaches. The proposed LFEA is employed to verify the proposed design optimization in previous section.

The LFEA consists of four basic steps, i.e., three-dimensional static magnetic analysis, defining layers and paths, data extraction, and data processing.

Firstly, the three-dimensional static magnetic analysis for the motor are carried out without post-processing. The procedure for doing such an analysis consists of the following main steps: create the physics environment, build and mesh the model, assign physics attributes to each region within the model, apply boundary conditions, and run the solver. Secondly, layers and paths are defined as shown in Fig. 5. The solved motor model is divided into layers equably along *y*-axis direction. The structure of each layer is considered to be steady when the number of layers is larger enough. A series of lines are formed by intersecting two vertical planes, the layers and the *x*-*y* working plane in the middle of air gap. These lines are defined as paths. Thirdly, the data, including the B_z and the longitudinal position along the defined paths, are extracted through sampling on the path and exported to files in ASCII formats. Finally, one can get the intuitive graphics by using the data from all layers and paths, like magnetic flux lines and the three-dimensional distribution of the B_z at the defined *x*-*y* working plane. The precision of LFEA depends on the number of layers and the number of samplings on the defined path.

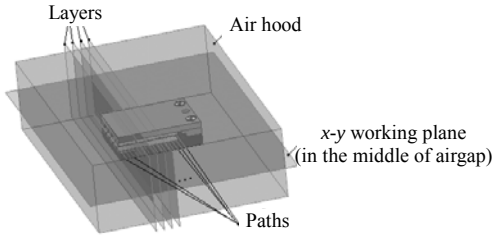

图 5 三维分层有限元法示意图

Fig. 5 Schematic diagram for LFEA

3.2 LFEA Solving

The motor is modeled with the optimized motor dimensions. The dimensions (length, width and height) of air hood should be three times as or more than those of the motor for the three-dimensional modeling. Since under this circumstances, the outer surface of air hood can be considered as the isosurface of magnetic potential .

Using LFEA, the 3D distribution of the B_z at the defined *x*-*y* working plane is shown in Fig. 6. There are some distortions due to the end effect and complex magnetic circuit relations. It can be seen the B_z is longitudinally sinusoidal and transversely uniform at the main working region, which is required for many precise positioning systems.

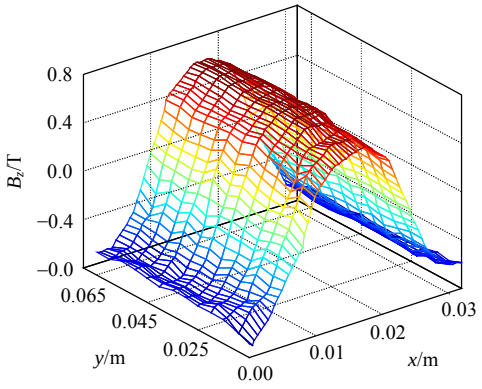

图 6 B_z 在定义平面上的分布

Fig. 6 The distribution of B_z at the *x*-*y* working plane

3.3 Comparison between layer model and LFEA

As mentioned above, we take the magnetic flux density stabilization as the primary problem. Thus, the distributions of B_z obtained by layer model and LFEA are compared to verify the LFEA.

Fig. 7 shows the distributions of B_z obtained by analytical layer model and LFEA along one defined path. It can be seen that the distributions of B_z obtained by analytical model and LFEA are in good agreement. The amplitude of air-gap magnetic flux density B_z obtained by LFEA is 0.760 5 T. The error is about 0.4% compared with that obtained by layer model, as shown in Tab. 5. It is within the allowable range. The result confirms the validity of the proposed LFEA. Furthermore, the results obtained by LFEA in previous subsection can confirm effectiveness of the proposed multiobjective optimization. And the distributions of B_z have a sinusoidal waveform with a 32 mm period, which is corresponding to the 2τ.

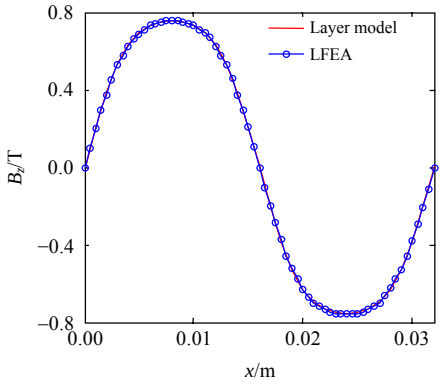

图 7　B_z 在定义路径上的分布

Fig. 7　Distribution of B_z along the defined path

表 5　不同方式得到的 B_z 峰值对比

Tab. 5　B_z Comparison among methods

Results	Layer model	LFEA	Experiment
Peak value of B_z/T	0.757 4	0.760 5	0.754 5

4　Experiment

4.1　Experiment setup

In the Precision Engineering Research Center at China Agricultural University, a motor prototype is manufactured with the optimized dimensions obtained above. Fig. 8 is the photograph of this UIPMLSM prototype. The NdFeB PM pieces are ordered from Beijign Topmag Magnet Co., Ltd. of grade N48 with the remanence B_r=1.38~1.40 T and the inside coercive force $H_{cj} \geq 955$ kA/m. The magnetic flux density B_z in the middle of air gap is detected using a SG-4L type digital teslameter with 1 μT resolution and 0.5% accuracy, which is bought from Beijing Zhuoshengjia Magnetic Technology Co., Ltd., China.

The experimental setup is shown in Fig. 9. The probe is set in the middle of air gap and the probe handle is fixed on a drive motor, as shown in Fig. 9(b). The probe moves together with the drive motor

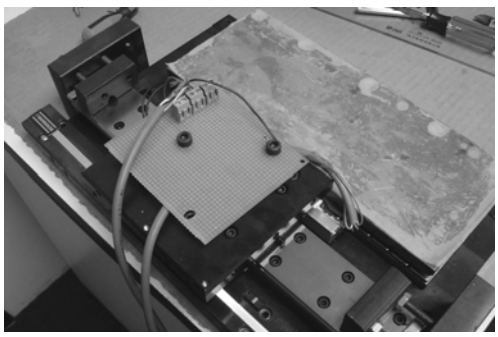

图 8　U 型永磁同步直线电机样机

Fig. 8　UIPMLSM prototype

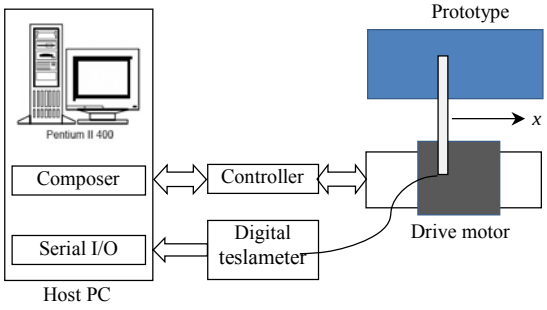

(a) 实验设置框图

(b) 实验设置实物图

图 9　实验设置

Fig. 9　Experimental setup

increased by 1 mm. The host PC sends motion command through Composer GUI of controller and records the position data. The air-gap magnetic flux density samplings are uploaded to the host PC through a RS-232 interface. Then, the air-gap magnetic flux density distribution can be generated.

4.2　Experiment results

The motor prototype flux density distribution in the middle of air gap is presented in Fig. 10. It can be easily seen the flux density distribution has a sinusoidal waveform with a period of 32 mm and amplitude of 0.754 5 T, as listed in the fourth column of Table 5. The ignorable differences among the amplitudes of B_z obtained by layer model, LFEA, and experiments are within the reasonable range. The differences originate from mainly the accuracy of the layer model, measurement noise and manufacturing reasons.

The Fourier transform is employed to find the amplitude spectrum of B_z. Fig. 11 is the Fourier transform result for the B_z distribution of motor prototype. It shows the proposed method has lower higher harmonic components which will reduce the force ripples of the motor. And it can be easily seen that the ratio of higher harmonics to whole wave is

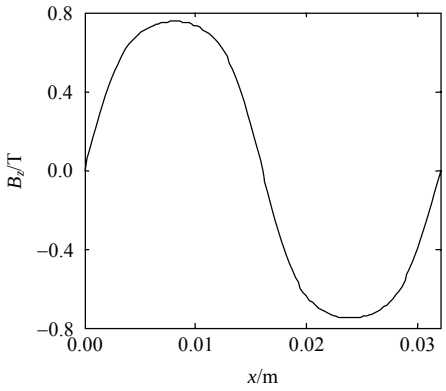

图 10 样机气隙中心的 B_z 分布

Fig. 10 B_z distribution of the prototype

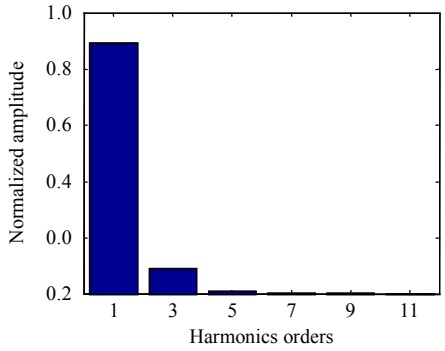

图 11 B_z 各次谐波频谱分布

Fig. 11 Normalized amplitude spectrum of B_z

less than 10.7%. These improvements further confirm the effectiveness of the proposed optimization.

5 CONCLUSION

This paper performs a multiobjective design optimization to a UIPMLSM. The optimization using GA yields excellent improvement in the thrust amplitude and reduction in the thrust ripple and magnetic material consumption. The optimized design is validated through LFEA and experimental results, which both demonstrated reasonable agreement with the analytical solution.

A layer model of the UIPMLSM with a fixed coil structure is introduced in defining the optimization problem. A multiobjective function is defined to increase amplitude of the air-gap magnetic flux density, reduce higher harmonics of the air-gap magnetic flux density distribution, and decrease the PM volume. The unrealistic results are prevented by limiting the design variables during optimization process. By choosing different relative importance, one can trade off several objectives in some way and achieve designer's specific issues. A GA is used to find the optimized PM dimensions and air-gap length with those appropriate constraints. Diversity is essential to the GA because it enables the algorithm to search a large region of the space. The LFEA is developed and employed to evaluate and confirm the validity of the design optimization. One can get lots of intuitive graphics using LFEA which is difficult in the 3DFEA. A motor prototype is manufactured with the optimized motor dimensions. Experimental results indicate that this optimization reduces magnetic flux density pulsations and magnet volume, while keeping relatively high amplitude of the sinusoidal air-gap magnetic flux density for the UIPMLSM simultaneously. The results we have obtained suggest that the magnetic flux density stabilization has a significant effect on the motor performance as the internal factor, as it contributes to the developed motor force directly. The improvement of magnetic flux density can improve the motor performance radically.

On the other hand, there are some external factors in practical operation, such as payload variation, unknown nonlinearities and disturbances. Thus, the connection of motor optimization designs and control strategies will produce the desired results to achieve the potential high performance for precise positioning systems.

参考文献

[1] Xu L，Yao B．Adaptive robust control of mechanical systems with nonlinear dynamic friction compensation [J]．International Journal of Control，2008，81(2)：167-176．

[2] Yao B．Advanced motion control: from classical PID to nonlinear adaptive robust control[C]//The 11th IEEE International Workshop on Advanced Motion Control．Nagaoka，Japan：IEEE，2010．

[3] Gieras J F，Piech Z J．Linear synchronous motors: transportation and automation systems[M]．Florida：CRC Press, 2000：5-15．

[4] Hong Y，Yao B．A globally stable high performance adaptive robust control algorithm with input saturation for precision motion control of linear motor drive system [J]．The IEEE/ASME Transactions on Mechatronics，2007，12(2)：198-207．

[5] Lu L，Yao B，Wang Q，Chen Z．Adaptive robust control of linear motors with dynamic friction compensation using modified LuGre model[J]．Automatica，2009，45(12)：2890-2896．

[6] Vaez-Zadeh S，Isfahani A H．Multiobjective design optimization of air-core linear permanent-magnet synchronous motors for improved thrust and low magnet consumption[J]．IEEE Transactions on Magnetics，2006，42(3)：446-452．

[7] Isfahani A H．Analytical framework for thrust enhancement in permanent-magnet (PM) linear synchronous motors with segmented PM poles[J]．IEEE Transactions on Magnetics，2010，46(4)：1116-1122．

[8] Kazan E，Onat A．Modeling of air core permanent-magnet linear motors with a simplified nonlineama rgnetic analysis[J]．IEEE Transactions on Magnetics，2011，47(6)：1753-1762．

[9] Vaez-Zadeh S，Isfahani A H．Enhanced modeling of linear permanent-magnet synchronous motors[J]．IEEE Transactions on Magnetics，2007，43(1)：746-749．

[10] Li Y，Xing J，Wang T，et al．Programmable design of magnet shape for permanent-magnet synchronous motors with sinusoidal back EMF waveforms[J]．IEEE Transactionsactions on Magnetics，2008，44(9)：2163-2167．

[11] Jang S，Lee S，Yoon I．Design criteria for detent force reduction of permanent-magnet linear synchronous motors with Halbach array[J]．IEEE Transactions on Magnetics，2002，38(5)：3261-3263．

[12] Lee M G，Lee S Q，Gweon D G．Analysis of Halbach magnet array and its application to linear motor[J]．Journal of Mechatronics，2004，14(1)：115-128．

[13] Li L，Na M，Kou B，et al．Analysis and optimization of slotless electromagnetic linear launcher for space use [J]．IEEE Transactions on Plasma Science，2011，39(1)：127-132．

[14] Tavana N R，Shoulaie A．Analysis and design of magnetic pole shape in linear permanent-magnet machine[J]．IEEE Transactions on Magnetics，2010，46(4)：1000-1006．

[15] Isfahani A H，Vaez-Zadeh S，Rahman M A．Using modular poles for shape optimization of flux density distribution in permanent-magnet machines[J]．IEEE Transactions on Magnetics，2008，44(8)：2009-2015．

[16] Zhu Z Q，Wu L J，Xia Z P．An accurate subdomain model for magnetic field computation in slotted surface-mounted permanent-magnet machines[J]．IEEE Transactions on Magnetics，2010，46(6)：1100-1115．

[17] Hosseini M S，Vaez-Zadeh S，Chen Z．Modeling and analysis of linear synchronous motors in high-speed maglev vehicles[J]．IEEE Transactions on Magnetics，2010，46(7)：2656-2664．

[18] Isfahani A H，Vaez-Zadeh S，Rahman M A．Performance improvement of permanent magnet machines by modular poles[J]．IET Electric Power Applications，2009，3(4)：343-351．

[19] Yang H S，Eum Y H，Zhang Yanli，et al．Multi-objective optimal design of a single phase AC solenoid actuator used foma rximum holding force and minimum eddy current loss[J]．Journal of Electrical Engineering & Technology，2008，3(2)：218-223．

[20] Zhou Z Q，Chen J T．Advanced flux-switching permanent magnet brushless machines[J]．IEEE Transactions on Magnetics，2010，46(6)：1447-1453．

[21] Zhang Yanli，Yuan Jingguo，Xie Dexin，et al．Shape optimization of a PMLSM using Kriging and genetic algorithm[C]//Proceedings of the 5th IEEE Conference on Industrial Electronics and Applications．Taichung，2010．

[22] Sun Peng，Zhou Huixing．Air-gap magnetic field design optimization for U-shaped ironless permanent magnet linear synchronous motors[C]//Proceedings of International Conference on Electrical Machines and Systems．Wuhan，China，2008．

[23] Chen X，Zhou Huixing，Ma Ronghua，et al．Linear motor driven inverted pendulum and lqr controller design[C]// Proceedings of International Conference on Automation and Logistics．Jinan，China，2007．

[24] Ma Ronghua，Zhou Huixing，Sun Peng，et al．dSPACE-based PID controller for a linear motor driven inverted pendulum[C]//Proceedings of International Conference on Mechatronics and Machine Vision in Practice．Xiamen，China，2007．

[25] 孙鹏，周惠兴．U 型无铁心永磁同步直线电机气隙磁场有限元分析及实验研究[J]．微电机，2009，42(8)：9-12，46．

Sun Peng，Zhou Huixing．Analysis and experimental research of air-gap magnetic field of U-shaped Ironless permanent magnet linear synchronous motor [J]．Micromotors，2009，42(8)：9-12，46(in Chinese).

孙鹏

收稿日期：2012-05-04。

作者简介：

孙鹏(1985)，男，博士研究生，主要从事直驱技术、磁场优化、自适应鲁棒控制方面的研究工作，sunpeng09@gmail. com；

周惠兴(1963)，男，教授，博士生导师，CEng, MIMechE, 主要从事现代数控机床技术、直驱技术、精密运动控制等方面的研究工作，hzhou@cau.edu.cn。

(责任编辑　王剑乔)